nature physics

LETTERS

https://doi.org/10.1038/s41567-019-0447-2

A primary radiation standard based on quantum nonlinear optics

Samuel Lemieux[1*], Enno Giese[1,6], Robert Fickler[1,7], Maria V. Chekhova[2,3,4] and Robert W. Boyd[1,5]

The black body remains the most prominent source of light for absolute radiometry[1]. Its main alternative, synchrotron radiation, requires costly and large facilities[2]. Quantum optics offers a new radiometric source: parametric down-conversion (PDC), a nonlinear optical process, in which pairwise photon correlations enable absolute calibration of photodetectors[3–6]. Since the emission rate crucially depends on the brightness of the electromagnetic field, quantum-mechanical fluctuations of the vacuum[7] can be seen as a seed of spontaneous PDC, and their amplitude is a natural radiometric standard. Thus, they allow for the calibration of the spectral radiance of light sources[8–11] by measuring the ratio between seeded and unseeded PDC. Here, we directly use the frequency spectrum of the electromagnetic vacuum to trigger spontaneous PDC and employ the generated light to infer the spectral response of a spectrometer over a broad spectral range. Then, we deduce the absolute quantum efficiency from the spectral shape of PDC in the high-gain regime, without relying on a seed or reference detector. Our results compare well with the ones obtained with a reference lamp, demonstrating a promising primary radiation standard.

In general, a source can serve as a primary radiation standard if, within a specified bandwidth centred on the wavelength λ, the exact number of emitted photons $N(\lambda)$ is known. However, the number of counts $M(\lambda)$ recorded by a detector does not usually coincide with $N(\lambda)$ due to an imperfect quantum efficiency $\eta(\lambda)$ of the detecting device. These quantities are simply connected through the relation

$$M(\lambda)=\eta(\lambda)N(\lambda) \tag{1}$$

Measuring $M(\lambda)$ while having a precise knowledge of $N(\lambda)$ allows the determination of $\eta(\lambda)$, which is at the heart of the absolute calibration of spectrometers. The spectral efficiency $\eta(\lambda)$ can be further separated into its relative spectral shape $R(\lambda)$ (that is, the response function of the measurement device) and a wavelength-independent proportionality constant α, through $\eta(\lambda)=\alpha R(\lambda)$. Whereas a relative calibration procedure gives $R(\lambda)$, obtaining the full $\eta(\lambda)$ requires an absolute calibration. In the following we demonstrate in a two-step procedure that both relative and absolute calibration can be performed using parametric down-conversion (PDC).

The total number of photons reaching the detector depends on the photon-number distribution $\mathcal{N}$ per plane-wave mode characterizing the source, and on the modes that are detected. Using standard radiometric formalism (see details in the Methods), this fact translates to the expression

$$\begin{aligned} N(\lambda) &= \frac{1}{(2\pi)^3}\int_{\text{source}} \mathrm{d}^3r \int_{\text{detector}} \mathrm{d}^3k\,\mathcal{N} \\ &\approx [A_s\ c\ \tau_s]\,[\Delta\Omega\Delta\lambda]\,\mathcal{D}(\lambda)\mathcal{N} \end{aligned} \tag{2}$$

where the first integral can be approximated by the transverse area A_s of the source and the duration of the emission τ_s multiplied by the speed of light c. The second integral describes the modes that are detected and can be approximated by the bandwidth $\Delta\lambda$ and solid angle $\Delta\Omega$ of the detector, if $\mathcal{N}$ does not vary significantly over these quantities. To connect the plane waves to the solid angle and the wavelength, which are the relevant quantities for a spectrometer, we also introduced the quantity $\mathcal{D}(\lambda)=(2\pi)^3\lambda^{-4}$, which is a measure of the mode density[7]. If $\mathcal{N}$ is known, we have all the necessary quantities for the absolute calibration of a spectrometer.

During the three-wave mixing process of PDC, pump photons (of frequency ω_p) interact with the vacuum field within a crystal with a nonlinear susceptibility $\chi^{(2)}$. This process leads to the generation of pairs of photons known as the signal and idler, of frequencies ω and ω_i. In the spontaneous regime (low pump intensity), $\mathcal{N}$, a function of frequency and emission angle, depends on the amplitude of the vacuum fluctuations, the profile of the pump beam, the gain of the amplification process and a phase-matching function. For a monochromatic plane wave pump of amplitude E_p and a crystal of thickness L, the photon-number spectral distribution of spontaneous PDC is given by

$$\mathcal{N}=(c^{-1}\,L\,\chi^{(2)}E_p)^2\sqrt{\omega\omega_i/(nn_i)^2}\,\mathrm{sinc}^2(\Delta\kappa L/2) \tag{3}$$

where n and n_i are the signal and idler refractive indices and $\Delta\kappa=\kappa_p-\kappa-\kappa_i$ is the mismatch between the longitudinal wavevectors of the pump, the signal and the idler, respectively[7,12]. The frequency-dependent factors $\sqrt{\omega/n}$ and $\sqrt{\omega_i/n_i}$ arise from the quantization of the electric field for the signal and for the idler[13]. In the spontaneous regime of pair creation, those factors embody the amplitude of the vacuum fluctuations for the biphoton field given by the density of states. They explicitly appear in the expression for the electric field operators for the signal and for the idler, which are used in turn to write the Hamiltonian for the nonlinear interaction. To denote the coupling strength, we use the gain parameter $\mathcal{G}=c^{-1}\,L\,\chi^{(2)}E_p/\sqrt{nn_i}$, which we can assume to be constant over

[1]Department of Physics, University of Ottawa, Ottawa, Ontario, Canada. [2]Max Planck Institute for the Science of Light, Erlangen, Germany. [3]Physics Department, Lomonosov Moscow State University, Moscow, Russia. [4]University of Erlangen-Nuremberg, Erlangen, Germany. [5]Institute of Optics, University of Rochester, Rochester, NY, USA. [6]Present address: Institut für Quantenphysik and Center for Integrated Quantum Science and Technology, Universität Ulm, Ulm, Germany. [7]Present address: Photonics Laboratory, Physics Unit, Tampere University, Tampere, Finland. *e-mail: samzlemieux@gmail.com

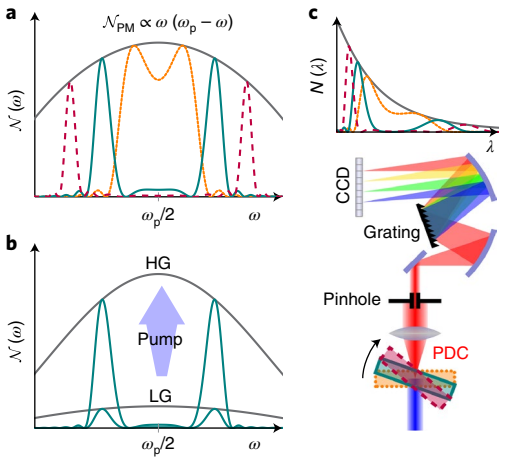

Fig. 1 | Physical principle and idealized set-up. a, Different tilt angles of the nonlinear crystal correspond to different phase-matching conditions, altering the spectrum $\mathcal{N}(\omega)$ accordingly, as exemplified by the orange, green and magenta curves. $\mathcal{N}_{PM}(\omega)$ (grey curve) is obtained by taking the maximum of $\mathcal{N}$ for different phase-matching conditions. Since the shape of $\mathcal{N}_{PM}(\omega)$ is known, see equation (4), we can use it as a reference to retrieve the response function $R(\lambda)$. **b**, The relative calibration with PDC is performed in the low-gain regime (LG) and the absolute calibration with PDC in the high-gain regime (HG). We transition from low gain to high gain by increasing the intensity of the pump laser. In the high-gain limit, there is a one-to-one correspondence between the shape of $\mathcal{N}_{PM}$ and the number of generated photons, leading to an absolute standard. **c**, For each tilt angle of the nonlinear crystal, the photon-number spectrum $N(\lambda)$ is measured with an angular filter (a pinhole in the far field selects a small solid angle) and a spectrometer. The shape of $N(\lambda)$ follows from the conversion of $\mathcal{N}(\omega)$ from the plane-wave representation to the wavelength and solid-angle representation associated with the spectrometer. CCD, charge-coupled device.

the frequency range of interest. This assumption is discussed in the Methods.

The last factor of equation (3) is the well-known phase-matching function of a bulk crystal. At exact phase-matching, $\Delta\kappa$ vanishes and the phase-matching function takes on the value unity. Thus, the phase-matched distribution (3) takes its maximal value and reads

$$\mathcal{N}_{PM} = \mathcal{G}^2\,\omega\,(\omega_p - \omega) \tag{4}$$

where we assumed that photon energy is conserved in the parametric process, such that $\omega_i = \omega_p - \omega$. For absolute calibration, we need a complete knowledge of $\mathcal{N}_{PM}$, but it is difficult to determine $\mathcal{G}$ experimentally in the spontaneous regime of PDC. However, the photon number for different $\mathcal{N}_{PM}$ follows a parabola, as illustrated in Fig. 1a. Because $\omega(\omega_p - \omega)$ does not depend on laboratory parameters, we use the shape of $\mathcal{N}_{PM}$ and perform a relative calibration[12].

By introducing a pinhole in the far-field of the crystal, we limit the emission solid angle and suppress the frequency content in the other angular modes (details in the Methods). A spectrometer then disperses the light and images it onto a charge-coupled device chip (see Fig. 1c). Since the position on the chip corresponds to a particular wavelength, we expect a specific functional behaviour that originates in the parabola but is modified by $\mathcal{D}(\lambda)$[14]. Thus, any deviation of the measured spectrum at the phase-matched wavelength from $\mathcal{D}(\lambda)\omega(\omega_p - \omega)$ can be assigned to detector inefficiencies, and therefore to $R(\lambda)$.

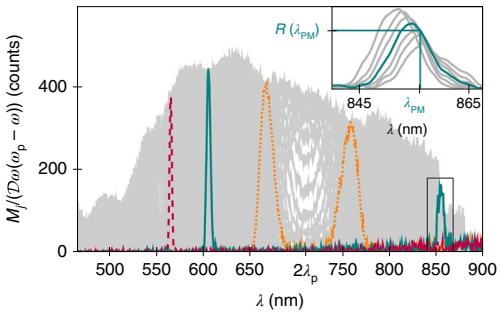

Fig. 2 | Measured spectra. We extract the response function $R(\lambda)$ from the overlap of 411 measured spectra (grey). The twin-peak structure in the orange and teal spectra is a feature of phase matching and energy conservation. For the magenta curve, the second peak does not lie within our measurement range. The maximum possible signal at a certain wavelength λ is proportional to $R(\lambda)$. To illustrate this method, the inset shows several spectra (Fourier-filtered to suppress the noise) from the box enclosing the right-hand peak of the teal curve.

Since $R(\lambda)$ is proportional to the ratio between the number of counts $M(\lambda)$ and the number of photons $N(\lambda)$, we can write

$$R(\lambda) \propto \left.\frac{M(\lambda)}{\mathcal{D}(\lambda)\omega(\omega_p - \omega)}\right|_{PM,LG} \tag{5}$$

where $\omega = 2\pi c/\lambda$ and we used the proportionality symbol because $\mathcal{G}$ is yet to be determined. The right-hand side is evaluated at the wavelength λ_{PM} that satisfies the phase-matching condition and the measured spectra $M(\lambda)$ are acquired in the low-gain limit, denoted by LG.

In our experiment, we pump a barium borate (BBO) crystal with a pulsed laser (355 nm wavelength) and acquire a large number of spectra M_j, with j corresponding to different tilt angles of the nonlinear crystal, spanning phase-matched frequencies over a broad spectral range, as shown at the bottom of Fig. 1c. We overlap all the measured spectra in Fig. 2 and highlight three of them to show their twin-peak structure. Crucially, the maximum number of counts at any particular wavelength as the crystal tilt angle is varied gives the phase-matched measurement $M_j(\lambda_{PM})$, because $\mathrm{sinc}^2(\Delta\kappa L/2)$ is equal to unity only when the phase-matching condition is satisfied. We show in the inset of Fig. 2 and in the Methods that the peak number of counts in a single spectrum does not always occur at λ_{PM}.

We perform the experiment in the spontaneous regime of PDC to ensure the validity of equation (3). We retrieve $R(\lambda)$ directly from the spectra by virtue of equation (5), where $M(\lambda_{PM})$ is extracted by taking the maximum of many spectra. We assume the normalization condition that for degenerate down-conversion $R(2\lambda_p) = 1$, such that $\eta(2\lambda_p) = \alpha$. The response function obtained from the spontaneous PDC agrees very well with the response function measured with a reference lamp (Fig. 3). The experiment was repeated with an additional dichroic filter to demonstrate that the method resolves rich and rapidly varying spectral features. For a proper comparison, it is crucial that the light from spontaneous PDC and from the reference lamp undergo exactly the same transfer function. The skewness of the PDC response with respect to that of the lamp stems from chromatic aberration and non-perfect polarization filtering, as well as inaccuracies in the reference spectrum of the lamp.

To improve the precision of our method, one could include the frequency dependence of $\mathcal{G}$ if the linear and nonlinear dispersion relations of the crystal are known. In this case, it is also straightforward to generalize equation (3) so that it incorporates the spatial

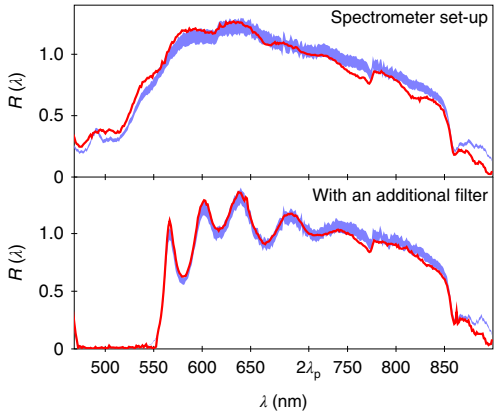

Fig. 3 | Spectral response function of the experimental set-up. Upper panel shows a comparison of $R(\lambda)$ obtained from spontaneous PDC (red, normalized to unity at the degenerate wavelength $2\lambda_p$) and the response function measured with a reference lamp (blue envelope enclosing the 5% error reported by the manufacturer; scaled onto the PDC curves using a linear fit). To obtain the curves in the lower panel, we added a dichroic filter to the spectrometer to induce rich spectral features into the response function.

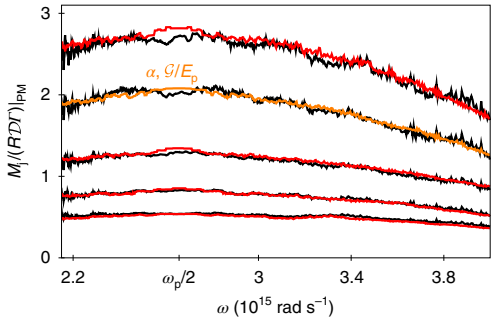

Fig. 4 | Absolute calibration from high-gain PDC. The maxima of densely packed high-gain spectra (right-hand side of equation (7); shown in black) and their fit (left-hand side of equation (7); shown in red and orange) are obtained for five different pump intensities. The curves are shown in the frequency domain to highlight the distortion of the parabola. The fit parameters for the orange curve were obtained with the second-to-top measurement. To demonstrate their accuracy, we used the same fit parameters to draw the red curves. The fitting curves are noisy because fluctuations in the pump energy are taken into account.

and temporal profiles of the pump beam[15]. To stress the simplicity of our procedure, we refrain from applying these corrections, but nonetheless obtain excellent results. With a knowledge of $R(\lambda)$ we can accurately measure the shape of any spectrum. In the following, we perform the second step of our calibration procedure and establish an absolute calibration method. In particular, we extract the number of photons from the shape of high-gain PDC spectra, based on our previous measurement of $R(\lambda)$, as exemplified in Fig. 1b, where we see a distortion of the parabola when the gain is increased.

For an arbitrary value of the gain, the photon-number spectral distribution under phase matching and for a monochromatic, plane-wave undepleted pump, becomes

$$\mathcal{N}_{PM} = \sinh^2\left(\mathcal{G}\sqrt{\omega\,(\omega_p-\omega)}\right) \tag{6}$$

which reduces to equation (4) in the spontaneous regime—that is, for $\mathcal{G}\sqrt{\omega\,(\omega_p-\omega)} \ll 1$[7]. In the high-gain regime, the phase-matched photon-number spectrum is therefore a distorted parabola, whose spectral shape (curvature) and photon number are uniquely determined by the gain parameter $\mathcal{G}$. In complete analogy to equation (5) we obtain the relation

$$\alpha\ \sinh^2\left(\mathcal{G}\sqrt{\omega\,(\omega_p-\omega)}\right) = \left.\frac{M(\lambda)}{R(\lambda)\mathcal{D}(\lambda)\Gamma}\right|_{PM} \tag{7}$$

where we introduced, for a more convenient notation, the constant $\Gamma = \Delta\Omega\Delta\lambda A_s c\tau_s$ for the emission and detection parameters. Note that, in contrast to equation (5), we have an equality. Except for α, which we defined earlier through $\eta(\lambda) = \alpha R(\lambda)$, all the quantities are known: we obtained $R(\lambda)$ from spontaneous PDC and the shape of the phase-matched spectrum uniquely determines $\mathcal{G}$. We approximate A_s by the transverse area of the pump beam and τ_s by $m\tau_p$, with τ_p being the pump pulse duration and m the number of pulses during an acquisition time. Further, we calculate the solid angle $\Delta\Omega$ from the pinhole size in the far field of the crystal, and obtain $\Delta\lambda$ from the bandwidth associated with a pixel of the spectrometer's camera. The only remaining free parameter, α, is obtained via fitting.

For that, we acquire a large number of densely packed spectra $M_j(\lambda)$ for different crystal tilt angles with a much higher pump energy per pulse to reach a large parametric gain. After taking the maxima of these dense spectra, we perform a bivariate curve fit using the free parameter α and the pump-normalized gain $\mathcal{G}/E_p$, a quantity that allows us to suppress the pulse energy drift of our pump laser over the acquisition time, and where a relative measurement of E_p is sufficient. We then obtain the spectral quantum efficiency by taking the product $\eta(\lambda) = \alpha R(\lambda)$, with R inferred from the spontaneous measurement and α from the high-gain regime.

In the absolute calibration measurement, we use a pump energy four times higher than in the spontaneous configuration. We show the maxima of the spectra and the fit (orange curve) in Fig. 4. The quantum efficiency at $\lambda = 2\lambda_p$, extracted from fitting, is $\alpha = 0.42 \pm 0.04$, where the uncertainty is dominated by the systematic error in the pulse duration and transverse profile of the pump. Note that α includes all the losses in the optical set-up, from the nonlinear crystal to the detector. The estimated quantum efficiency of the experimental set-up, based on the nominal efficiency of each optical component, is $\alpha = 0.38 \pm 0.07$. The largest source of loss is the diffraction grating of the spectrometer, with an efficiency of 60% at $2\lambda_p$, as reported by the manufacturer. In addition, we tested the consistency of the fit parameters by repeating the measurement with other pump energies. Using the previously obtained value of α, and estimating the gain from $\mathcal{G}/E_p$ and a new measurement of E_p, we obtain the red curves (Fig. 4), which also show excellent agreement with experimental data. Undesired effects due to additional nonlinear processes arising with the higher pump intensity, such as self-focusing or fluorescence, are found to be negligible.

Equation (6) is obtained by solving the Heisenberg equation of motion for the creation and annihilation operators in the form of a Bogolyubov transformation relating the modes associated with the signal and the idler photons[7]. The validity of models for high-gain PDC in the context of a pulsed laser has been discussed[16] and verified experimentally by looking at the exponential increase in the number of photons with the pump power[14,17–20]. The results presented in Fig. 4 are experimental demonstrations of the distortion of the phase-matched spectral shape of light generated by a pulsed laser for increasing gain, and as such provide additional support for this description of PDC. Moreover, equation (7) underlines that high-gain PDC offers the possibility to perform the absolute calibration of a single-element detector by measuring the number of counts against the pump pulse energy.

In contrast to the relative calibration, the absolute calibration using high-gain PDC cannot be straightforwardly generalized to arbitrary pump beams. Corrections to the model could be implemented, for instance by taking into account the spatial profile and frequency spectrum of the pump as well as the frequency dependence of $\mathcal{G}$. However, our results demonstrate that even without a more sophisticated treatment, which would require the determination of many more laboratory parameters and solving Heisenberg's equations of motion numerically, we measure the quantum efficiency accurately. State-of-the-art spectroradiometric sources based on black-body radiation, which have benefited from a century of technical improvements, typically exhibit a relative uncertainty of the order of 1% around the wavelength 700 nm (ref. [21]), whereas we report a relative uncertainty of the order of 10%. It is reasonable to expect that a PDC standard could reach the level of precision of methods based on black-body radiation. As a first step, one could carefully monitor the pump laser spatial profile and pulse duration. Less prominent sources of error, which include geometric factors and the quality of the fitting, could also be addressed. Furthermore, it would be interesting to explore different strategies to engineer the density of states, by using for instance metallic surfaces or nanoparticles, to increase the brightness of the source.

Online content

Any methods, additional references, Nature Research reporting summaries, source data, statements of data availability and associated accession codes are available at https://doi.org/10.1038/s41567-019-0447-2.

Received: 13 August 2018; Accepted: 24 January 2019;
Published online: 04 March 2019

References

1. Hollandt, J. et al. in *Optical Radiometry: Volume 41 (Experimental Methods in the Physical Sciences)* (eds Parr, A. C. et al.) Ch. 5 (Elsevier, Amsterdam, 2005).
2. Lemke, D. & Labs, D. The Synchrotron Radiation of the 6-GeV DESY Machine as a Fundamental Radiometric Standard. *Appl. Opt.* **6**, 1043–1048 (1967).
3. Klyshko, D. N. Use of two-photon light for absolute calibration of photoelectric detectors. *Sov. J. Quantum Electron.* **10**, 1112–1117 (1980).
4. Malygin, A. A., Penin, A. N. & Sergienko, A. V. Absolute calibration of the sensitivity of photodetectors using a biphotonic field. *JETP Lett.* **33**, 477–480 (1981).
5. Polyakov, S. V. & Migdall, A. L. High accuracy verification of a correlated-photon-based method for determining photon-counting detection efficiency. *Opt. Express* **15**, 1390–1407 (2007).
6. Rarity, J. G., Ridley, K. D. & Tapster, P. R. Absolute measurement of detector quantum efficiency using parametric downconversion. *Appl. Opt.* **26**, 4616–4619 (1987).
7. Klyshko, D. N. *Photons and Nonlinear Optics* (Gordon and Breach, Boca Raton, 1989).
8. Klyshko, D. N. Utilization of vacuum fluctuations as an optical brightness standard. *Sov. J. Quantum Electron.* **7**, 591–595 (1977).
9. Kitaeva, G. Kh., Penin, A. N., Fadeev, V. V. & Yanait, Yu. A. Measurement of brightness of light fluxes using vacuum fluctuations as a reference. *Sov. Phys. Dokl.* **24**, 564–566 (1979).
10. Migdall, A., Datla, R., Sergienko, A., Orszak, J. S. & Shih, Y. H. Measuring absolute infrared spectral radiance with correlated visible photons: technique verification and measurement uncertainty. *Appl. Opt.* **37**, 3455–3463 (1998).
11. Kornienko, V. V., Kitaeva, G. Kh., Sedlmeir, F., Leuchs, G. & Schwefel, H. G. Towards terahertz detection and calibration through spontaneous parametric down-conversion in the terahertz idler-frequency range generated by a 795 nm diode laser system. *APL Photon.* **3**, 051704 (2018).
12. Lemieux, S. et al. Engineering the frequency spectrum of bright squeezed vacuum via group velocity dispersion in an SU(1, 1) interferometer. *Phys. Rev. Lett.* **117**, 183601 (2016).
13. Milonni, P. Field quantization and radiative processes in dispersive dielectric media. *J. Mod. Opt.* **42**, 1991–2004 (1995).
14. Spasibko, K. Yu, Iskhakov, T., Sh. & Chekhova, M. V. Spectral properties of high-gain parametric down-conversion. *Opt. Express* **20**, 7507–7515 (2012).
15. Hsu, F.-K. & Lai, C.-W. Absolute instrument spectral response measurements using angle-resolved parametric fluorescence. *Opt. Express* **21**, 18538–18552 (2013).
16. Dayan, B. Theory of two-photon interactions with broadband down-converted light and entangled photons. *Phys. Rev. A* **76**, 043813 (2007).
17. Agafonov, I. N., Chekhova, M. V. & Leuchs, G. Two-color bright squeezed vacuum. *Phys. Rev. A* **82**, 011801 (2010).
18. Allevi, A. et al. Coherence properties of high-gain twin beams. *Phys. Rev. A* **90**, 063812 (2014).
19. Brida, G., Meda, A., Genovese, M., Predazzi, E. & Ruo-Berchera, I. Systematic study of the PDC speckle structure for quantum imaging applications. *J. Mod. Opt.* **56**, 201–208 (2009).
20. Pérez, A. M. et al. Bright squeezed-vacuum source with 1.1 spatial mode. *Opt. Lett.* **39**, 2403–2406 (2014).
21. Yoon, H. W., Gibson, C. E. & Barnes, P. Y. Realization of the National Institute of Standards and Technology detector-based spectral irradiance scale. *Appl. Opt.* **41**, 5879–5890 (2002).

Acknowledgements

We thank O. Reshef for valuable discussions. This research was performed as part of a collaboration within the Max Planck-University of Ottawa Centre for Extreme and Quantum Photonics, whose support we gratefully acknowledge. This work was supported by the Canada First Research Excellence Fund award on Transformative Quantum Technologies and by the Natural Sciences and Engineering Council of Canada (NSERC). R.F. acknowledges the financial support of the Banting postdoctoral fellowship of the NSERC and S.L. the financial support from Le Fonds de Recherche du Québec Nature et Technologies.

Author contributions

M.V.C. conceived the idea for relative calibration. S.L., E.G. and R.F. extended that idea to the absolute calibration scheme. S.L. and R.F designed the experiment. S.L. conducted the experiment and performed the data analysis. S.L., E.G. and R.F. wrote the manuscript. M.V.C. and R.W.B. supervised the project. All authors contributed to scientific discussions.

Competing interests

S.L., M.V.C. and R.W.B., along with coinventors M. Manceau and G. Leuchs, the University of Ottawa and the Max Planck Institute for the Science of Light, have an international patent application (PCT/IB2017/056450) currently pending, about the relative calibration using PDC. E.G. and R.F. declare that they have no competing interests.

Additional information

Supplementary information is available for this paper at https://doi.org/10.1038/s41567-019-0447-2.

Reprints and permissions information is available at www.nature.com/reprints.

Correspondence and requests for materials should be addressed to S.L.

Publisher's note: Springer Nature remains neutral with regard to jurisdictional claims in published maps and institutional affiliations.

© The Author(s), under exclusive licence to Springer Nature Limited 2019

Methods

Radiometry. Since the quantization of the electric field is usually performed in plane-wave modes denoted by a wavevector $\mathbf{k}$, we express general radiometric quantities through the photon number per mode $\mathcal{N}(\mathbf{k})$ of the field under consideration. A detector cannot detect all of these modes, and hence the detected photon number per source volume can be written as

$$\varrho = \frac{1}{(2\pi)^3}\int_{\text{detector}} \mathrm{d}^3k\,\mathcal{N}(\mathbf{k}) = \int_{\Delta\lambda}\mathrm{d}\lambda\int_{\Delta\Omega}\mathrm{d}\Omega\,\frac{1}{\lambda^4}\mathcal{N}(\mathbf{k}) \tag{8}$$

where we used $\mathrm{d}^3k = k^2\mathrm{d}k\mathrm{d}\Omega = (2\pi)^3\lambda^{-4}\mathrm{d}\lambda\mathrm{d}\Omega$ in the last step. We neglect here the index of refraction of air and assume that the detector has a bandwidth of $\Delta\lambda$ and collects light from a solid angle $\Delta\Omega$. In the following we introduce for a more convenient notation the Jacobian $\mathcal{D}(\lambda) = (2\pi)^3\lambda^{-4}$, relating d^3k and $\mathrm{d}\lambda\mathrm{d}\Omega$, which is proportional to the mode density. For a sufficiently small $\Delta\lambda$ around the wavelength λ and a small $\Delta\Omega$ around the direction set by $\mathbf{k}$, we can perform the integration and find

$$\varrho(\lambda,\Omega) \cong \frac{1}{(2\pi)^3}[\Delta\lambda\Delta\Omega]\,\mathcal{D}(\lambda)\mathcal{N}(\mathbf{k}) \tag{9}$$

This quantity is closely related to the spectral radiance $\hbar\omega(2\pi)^{-3}c\mathcal{D}(\lambda)\mathcal{N}$, which is the energy per unit of time, area of the source, solid angle and bandwidth (in wavelength) of the detector[22].

To calculate the total number of photons that fall onto the detector, equation (9) has to be integrated over the volume of the source, to obtain

$$N(\lambda,\Omega) = \int_{\text{source}} \mathrm{d}^3r\;\varrho(\lambda,\Omega) \cong (2\pi)^{-3}[A_s c\tau_s]\,[\Delta\lambda\Delta\Omega]\,\mathcal{D}(\lambda)\mathcal{N} \tag{10}$$

where in the last step we assumed that the source has a surface area of A_s and emits light for a time duration τ_s.

We have not yet specified $\mathcal{N}(\mathbf{k})$. We do that in the next section and show that the assumption of a small solid angle as well as a small bandwidth of the detector is justified.

Angular distribution of spontaneous PDC. The photon number per mode $\mathcal{N}$ for spontaneous PDC in a bulk crystal of length L with a nonlinearity $\chi^{(2)}$ and illuminated by a plane wave pump with a field amplitude E_p is given by equation (3). The longitudinal wavevectors appearing in the expression for $\Delta\kappa$ are given by $\kappa \equiv \sqrt{k^2 - \mathbf{q}^2}$ for the signal and $\kappa_i \equiv \sqrt{k_i^2 - \mathbf{q}_i^2}$ for the idler. Here, the signal and idler photons have the wavevectors k and k_i and the transverse wavevectors $\mathbf{q}$ and $\mathbf{q}_i$. Note that $k_j = \omega_j n_j/c$, with c the speed of light and ω_j the frequency of the idler and pump fields with j = i,p, and no subscript for the signal.

With this notation, we find the expression

$$\Delta\kappa = k_p - \kappa - \sqrt{k_i^2 - \mathbf{q}_i^2} \tag{11}$$

for the longitudinal wavevector mismatch. Since we assume in equation (3) a plane wave and monochromatic pump, we have due to energy conservation $\omega_i = \omega_p - \omega$ and due to momentum conservation $\mathbf{q} = -\mathbf{q}_i$. Hence, our expression depends only on ω and $\mathbf{q}$. Moreover, introducing spherical coordinates, we can define the polar angle θ of the detected field and have $\cos\theta = \kappa/k$ and $\sin\theta = |\mathbf{q}|/k$. Therefore, the longitudinal wavevector mismatch

$$\Delta\kappa = k_p - k\left(\cos\theta + \sqrt{(k_i/k)^2 - \sin^2\theta}\right) \tag{12}$$

as well as equation (3), depends only on λ (using $\omega = 2\pi c/\lambda$) and θ, which are the natural dimensions of the detector.

In equation (9) we approximated the integral of $\mathcal{N}$ over $\mathrm{d}\lambda$ and $\mathrm{d}\Omega = \sin\theta\mathrm{d}\theta\mathrm{d}\phi$ by just multiplying the integration intervals. This is of course valid if $\mathcal{N}$ depends only weakly on both λ and θ over the range of interest.

In the experiment we place a pinhole in the far field of the spontaneous PDC light to filter a small range of angles. We show in the density plot of Supplementary Fig. 1 the product $\mathcal{D}(\lambda)\mathcal{N}$ as a function of θ and λ, and mark the size of our pinhole by a semi-transparent white strip. This numerical result is based on the Sellmeier equations of the three fields for BBO[23]. We further assume that $\mathcal{G}$ is constant in the wavelength range of interest, and we justify this assumption in the next section. We work close to collinear propagation, with $\theta \approx 0$, where the function $\mathcal{D}(\lambda)\mathcal{N}$ does not vary significantly across the pinhole area so that we can perform the integration by just multiplying by the solid angle. Similarly, the size of a pixel corresponds roughly to a bandwidth of 0.063 nm. On this scale, $\mathcal{N}$ does not change significantly. Hence, our approximation in equation (9) is valid for our set-up.

Of course, one can also integrate over the solid angle covered by the pinhole to obtain a more accurate result, but at some point the contribution of other crystal properties, such as its length, as well as the dispersion relations of all the light fields will dominate. In the spirit of an easy-to-implement calibration technique, we refrain from this more complex analysis but emphasize that it is possible. In a similar manner, one could include both the frequency as well as the angular profile of the pump in equation (3). However, on axis this treatment would not lead to a different result and our plane wave and monochromatic assumption is well-justified for our laser system.

Wavelength dependence of gain. In the main text, we assumed that the wavelength dependence of the gain function

$$\mathcal{G} = c^{-1}L\chi^{(2)}E_p \,/\, \sqrt{nn_i} \tag{13}$$

can be neglected. In this section, we investigate different effects that could contribute to the wavelength dependence in our experiment and demonstrate that they do not vary much across the spectral region of interest. In addition to the linear dispersion ($n(\lambda)$ and $n_i(\lambda)$) as well as the nonlinear dispersion $\chi^{(2)}(\omega_p, \omega, \omega_i)$, obvious from equation (13), other contributions arise from tilting the angle of the crystal to scan different phase-matching conditions. By tilting the crystal, the Fresnel coefficients vary (for the pump or for the down-converted light) and the effective length L of the nonlinear crystal (defined as the length of propagation of the pump inside the crystal) changes. The different Fresnel coefficients change the intensity of the pump inside the crystal, as well as how much of the down-converted light couples out of the crystal. Using the Sellmeier equations for BBO[23] and Miller's rule[24] (relating the first-order and second-order susceptibilities), we estimate the impact of those contributions, and show our results in Supplementary Fig. 2. The largest deviations are attributed to the dispersion in the nonlinear susceptibility $\chi^{(2)}$ and to the change in the effective length of the nonlinear crystal upon tilting it. However, over a spectral range of 300 nm around degeneracy, the gain function $\mathcal{G}$ does not vary by more than 1%.

Experimental set-up. A detailed set-up is shown in Supplementary Fig. 3. The third harmonic (355 nm wavelength, 29 ps pulse duration, 50 Hz repetition rate, pump beam area $A_s = 2\pi\sigma^2 = (0.17 \pm 0.01)\,\mathrm{mm}^2$, with the standard deviation σ of the Gaussian profile, 100 µJ pulse energy in the spontaneous regime, up to 500 µJ in the high-gain regime) of a pulsed Nd:YAG laser (EKSPLA, PL2231) is prepared as the pump for PDC from a nonlinear crystal (β-BBO, 3 mm thickness, type-I phase-matching, uncoated, cut for degenerate PDC) whose phase-matching frequencies are tuned using a motorized rotation mount. We estimate the systematic error on the pulse duration to be ± 2 ps. The standard error on the pump beam area is obtained from repeated measurements of the attenuated pump on the Gentec Beamage-3.0 beam profiler. The wavelengths that satisfy the phase-matching condition are tuned by varying the angle between the optic axis of the crystal and the wavevector of the pump. We test the uniformity of the crystal by measuring the PDC spectra produced by pumping different portions of the crystal. A set of dichroic mirrors removes the pump after the crystal. The pump energy drift over time is monitored using a photodiode. A concave mirror of focal length 200 mm is used to bring the down-converted light to the far field, where a pinhole (0.5 mm diameter) selects a small solid angle. To ensure a fixed polarization, a broadband polarizing beam splitter is placed before the pinhole. A pair of lenses is used to image the pinhole onto the entrance slit (1 mm in width) of the spectrometer with a magnification of 4/3. The spectrometer is an imaging spectrograph (Acton SP-2558) with a charge-coupled device camera (PIXIS:100BR_eXcelon, pixels of size 20 µm × 20 µm). Transverse binning is enabled, so that the signal at a certain wavelength is the sum of the photoelectron counts over all the pixels that correspond to that wavelength. The integration time for each of the 411 spectra is 500 ms. Each spectrum spans the range from 450 nm to 900 nm. To cover this range, we need to repeat the acquisition for different angular positions of the grating (600 grooves per mm, 500 nm blaze). The experiment is automated: after each acquisition by the spectrometer, the motorized holder rotates the crystal through an angle of about 0.01°, up to a total change of approximately 8°. To reduce errors, we filter out the noise (rapidly fluctuating signal) in each spectrum with an algorithm based on the fast Fourier transform. For the nonlinear curve fitting of PDC in the high-gain regime, we used a weight function to reduce the influence of the data points associated with high residuals. The spectrometer is calibrated in wavelength using a neon–argon lamp along with a Princeton Instruments Intellical system. The reference lamp (an LED-stack with a diffuser, Princeton Instruments) is introduced at the crystal plane. Its spectrum is acquired using the same experimental settings.

Details of the data analysis. Our calibration method relies on the comparison of the measured phase-matched number of counts $M(\lambda_{PM})$ to the expected phase-matched number of photons $N(\lambda_{PM})$. We therefore acquire a large number of spectra M_j corresponding to different phase-matching conditions over a broad spectral range. However, the peak number of counts in a measured spectrum does not correspond, in general, to $M(\lambda_{PM})$. Instead, we can extract the response function from the properties of $\mathcal{N}$. From the main text, we know that

$$\mathcal{N} \propto \omega(\omega_p - \omega)\,\mathrm{sinc}^2(\Delta\kappa L/2) \leq \omega(\omega_p - \omega) \tag{14}$$

where the inequality becomes an equality only for phase matching $\Delta\kappa = 0$. We denote the wavelength of phase matching with λ_{PM}. With equation (5) we find the inequality

$$R(\lambda) \geq R(\lambda)\mathrm{sinc}^2\frac{\Delta\kappa L}{2} \propto \frac{M_j(\lambda)}{\mathcal{D}(\lambda)\omega(\omega_p-\omega)} \tag{15}$$

with an equality sign for $\lambda = \lambda_{PM}$. If we approximate the phase matching function by a Gaussian, that is,

$$\mathrm{sinc}^2(\Delta\kappa L\,/\,2) \propto \exp\left[-(\lambda-\lambda_{PM})^2\,/\,(2\sigma_\lambda^2)\right] \tag{16}$$

it is easy to show that the peak of the product $R(\lambda)\mathrm{sinc}^2(\Delta\kappa L/2)$ shifts to the wavelength

$$\tilde{\lambda} = \lambda_{PM} + \frac{1}{R}\frac{\mathrm{d}R}{\mathrm{d}\lambda}\bigg|_{\tilde{\lambda}}\sigma_\lambda^2 \tag{17}$$

Hence, the steeper the slope of the response function, the greater the shift between the phase-matched wavelength and the peak. We show this effect in the inset of Fig. 2. Since the response function is not known but is the result of the calibration procedure, equation (17) cannot be used to determine the phase-matching wavelength. However, equation (15) directly gives a method to determine the response function despite the shift: when we acquire a large number of spectra M_j, each with a slightly varying λ_{PM}, the amplitude of $M_j\,/\,[\mathcal{D}\omega(\omega_p-\omega)]$ at one particular wavelength is the largest if the wavelength corresponds to λ_{PM}. Hence, we obtain the response function from

$$R(\lambda) = \max_j\left[\frac{M_j(\lambda)}{\mathcal{D}(\lambda)\omega(\omega_p-\omega)}\right] \Big/ \max_j\left[\frac{4M_j(2\lambda_p)}{\mathcal{D}(2\lambda_p)\omega_p^2}\right] \tag{18}$$

where we normalize the response function to unity at the degenerate wavelength $\lambda = 2\lambda_p$. To reduce errors in the analysis according to equation (18), we suppress for each spectrum $M_j(\lambda)$ the high-frequency content, filtered out via a fast Fourier transform procedure.

A similar idea can be used for absolute calibration. For an arbitrary $\mathcal{G}$, the photon distribution per plane-wave mode assuming a monochromatic plane wave pump can be written as[7]

$$\mathcal{N}^{(\mathrm{HG})} = \frac{\mathcal{G}^2\mathcal{Q}^2}{\mathcal{G}^2\mathcal{Q}^2-(\Delta\kappa L\,/\,2)^2}\sinh^2\sqrt{\mathcal{G}^2\mathcal{Q}^2-(\Delta\kappa L\,/\,2)^2} \tag{19}$$

where $\mathcal{Q}^2 \equiv \omega(\omega_p-\omega)$ and the superscript (HG) highlights that we are using this equation to describe the high-gain regime of PDC. Since the maximum of this function occurs for phase matching ($\Delta\kappa = 0$), we find

$$\mathcal{N}^{(\mathrm{HG})} \leq \sinh^2(\mathcal{G}\mathcal{Q}) \equiv \mathcal{N}_{\mathrm{PM}}^{(\mathrm{HG})} \tag{20}$$

where we defined the phase-matched photon distribution $\mathcal{N}_{\mathrm{PM}}^{(\mathrm{HG})}$, which has the well-known hyperbolic form of parametric amplification and is used in the main body of our article. Note further that for $\mathcal{G}\mathcal{Q} \ll 1$ we recover the low-gain result.

The quantum efficiency at the degenerate wavelength $\alpha = \eta(2\lambda_p)$ is

$$\alpha = M_j(\lambda)/\,[R(\lambda)N(\lambda)] \tag{21}$$

with the definitions from the main text. With that, we find from equation (20) and with the help of equation (10) the inequality

$$\alpha\,\sinh^2\mathcal{G}\mathcal{Q} \geq M_j(\lambda)/\,[R(\lambda)\mathcal{D}(\lambda)\Delta\Omega\Delta\lambda A_s c\tau_s] \tag{22}$$

where again the equal sign is valid for $\lambda = \lambda_{PM}$. Hence, we find, similarly to the low-gain method

$$\alpha\,\sinh^2\mathcal{G}\mathcal{Q} = \max_j\left[\frac{M_j(\lambda)}{R(\lambda)\mathcal{D}(\lambda)\Delta\Omega\Delta\lambda A_s c\tau_s}\right] \tag{23}$$

as an exact equality if the spectra are sufficiently dense. Taking the maximum of all recorded spectra, each one of them divided by $R(\lambda)\mathcal{D}(\lambda)$ and a numerical factor that depends on laboratory parameters (spatial dimensions and bandwidths), we can fit the data to the function $\alpha\,\sinh^2\mathcal{G}\mathcal{Q}$ with two fitting parameters α and $\mathcal{G}$. Note that we do not need to measure the exponential increase of the number of generated photons with increasing pump intensity, but determine both parameters from the distortion of the spectral shape of the maximum of all spectra. With this fitting procedure, one can determine not only the quantum efficiency $\eta(\lambda) = \alpha R(\lambda)$, but also the gain $\mathcal{G}$.

Even though we do not use the exponential increase with the pump power for our calibration method, we still record the intensity while scanning different phase matching functions. We do this to correct for drifts and fluctuations during the course of one measurement. We are then able to perform the fitting procedure using $\mathcal{G}\,/\,E_j$, where E_j is the pump field amplitude during measurement corresponding to the jth phase-matching condition.

The α obtained using our method for absolute calibration is compared to an estimated quantum efficiency based on the properties of each optical component in the experimental set-up, listed in Supplementary Table 1. The losses of uncoated components are estimated from the Fresnel coefficients, whereas the losses of coated components are taken from the manufacturers.

Spontaneous regime of PDC. As shown in equation (19), the photon-number distribution grows exponentially with the intensity of the pump. In the low-gain regime, where the photon pairs are generated spontaneously, the number of photons grows linearly with the intensity, which can be seen from the expansion

$$\mathcal{N}_{\mathrm{PM}}^{(\mathrm{HG})} = \sinh^2\mathcal{G}\mathcal{Q} \cong \mathcal{G}^2\mathcal{Q}^2 = \mathcal{G}^2\omega(\omega_p-\omega) = \mathcal{N}_{\mathrm{PM}} \tag{24}$$

where $\mathcal{N}_{\mathrm{PM}}$ is the low-gain photon distribution for phase matching. To obtain the response function $R(\lambda)$, we do not need to know the exact value of $\mathcal{G}$, but rely on the fact that the first-order expansion above is valid. Note that $\mathcal{G}^2$ is proportional to the intensity of the pump[7]. To verify that we work in the spontaneous regime of PDC, we measure the number of counts for a single wavelength and increase the pump intensity. The results, given in Supplementary Fig. 4, show that we are well within the linear regime up to roughly 150 μJ pump energy. We performed the relative calibration experiment at a pump intensity of 100 μJ, whereas the high-gain part of the experiment used a more intense pump, around 200 μJ and higher.

Data availability

The data that support the plots within this paper and other findings of this study are available from the corresponding author on reasonable request.

References

22. Datla, R. U. & Parr, A. C. in *Optical Radiometry: Volume 41 (Experimental Methods in the Physical Sciences)* (eds Parr, A. C. et al.) Ch. 1 (Elsevier, Amsterdam, 2005).
23. Eimerl, D., Davis, L., Velsko, S., Graham, E. K. & Zalkin, A. Optical, mechanical, and thermal properties of barium borate. *J. Appl. Phys.* **62**, 1968–1983 (1987).
24. Boyd, R. W. *Nonlinear Optics* (Academic, Burlington, 2003).